

THE INFLUENCE OF DYNAMIC INFLOW AND TORSIONAL FLEXIBILITY ON ROTOR DAMPING
IN FORWARD FLIGHT FROM SYMBOLICALLY GENERATED EQUATIONS

T. S. R. Reddy
National Research Council Research Associate

and

William Warmbrodt
Aerospace Engineer

NASA Ames Research Center
Moffett Field, California

Abstract

The combined effects of blade torsion and dynamic inflow on the aeroelastic stability of an elastic rotor blade in forward flight are studied. The governing sets of equations of motion (fully nonlinear, linearized, and multiblade equations) used in this study are derived symbolically using a program written in FORTRAN. Stability results are presented for different structural models with and without dynamic inflow. The study shows that symbolic and numerical programs written in FORTRAN can be conveniently used in a complicated helicopter-rotor aeroelastic modeling and analytical process. It is observed that for a large number of degrees of freedom and for fully nonlinear models, the amount of data needed for the symbolic program increases exponentially, making it inconvenient to consider the multiblade equations explicitly. However, a combination of symbolic and numerical programs at the proper stage in the derivation process makes the obtainment of final stability results an efficient and straightforward procedure. The symbolically generated equations are subsequently used to investigate the influence of elastic torsion modes and dynamic inflow on isolated rotor inplane stability in forward flight. Results are presented for both single-rotor-blade models and multiblade rotor systems. For both soft inplane and stiff inplane hingeless rotors, the elastic torsion mode significantly affects the predicted inplane damping. Dynamic inflow does change the magnitude of the predicted damping, but the influence on damping trends is generally small with varying advance ratio or elastic coupling parameter.

Notation

a = lift-curve slope, $2\pi/\text{rad}$
 b = number of blades

Presented at the Second Decennial Specialists' Meeting on Rotorcraft Dynamics, Ames Research Center, Moffett Field, California, November 7-9, 1984.

c = chord, m
 C_{d_0} = profile drag coefficient
 C_{mx}, C_{my} = rotor steady pitch and roll moments, Eq. (11)
 \bar{C}_T, C_H, C_W = rotor steady thrust, drag force, and weight coefficient, Eq. (11)
 C_T, C_M, C_L = harmonic perturbation coefficients of thrust, pitching moment, and rolling moment, Eq. (3)
 D = partial derivative matrix, Eq. (14)
 \bar{f} = flat-plate area
 F = forcing function, Eq. (6)
 J = number of points used in harmonic analysis, Eq. (5)
 K_A = blade cross-section polar radius of gyration, m
 K_m = blade cross-section mass radius of gyration, m
 K_{m1}, K_{m2} = principal mass radii of gyration, m
 L = number of harmonics used in the harmonic analysis, Eq. (10)
 $[m], [l]$ = dynamic inflow matrices
 $[M], [C], [K]$ = constant mass, damping, and stiffness matrices, Eq. (6)
 n = number of the harmonics in harmonic analysis, Eq. (9)
 N = total number of blade modes used
 q = perturbation degrees of freedom, Eq. (15)
 q_0, p_c, q_s = vectors of collective and cyclic modes, respectively
 R = rotor radius, m

u = dynamic inflow quantities, Eq. (19)
 U_T, U_P = tangential and perpendicular velocity components, m/sec
 v_i = induced velocity
 w, v, ϕ = flap, lag, and torsion deflections
 $\bar{w}, \bar{v}, \bar{\phi}$ = steady flap, lag, and torsion deflections, Eq. (2)
 x = blade coordinate along the radius
 z = first-order variable degrees of freedom, Eq. (15)
 α = rotor-shaft plane angle of attack, Eq. (11)
 α_R = wake skew angle, Eq. (4)
 β_{PC} = precone angle, rad
 γ = Lock number
 $\Delta w, \Delta v, \Delta \phi$ = perturbation flap, lag, and torsion deflections, Eq. (2)
 ζ_K, ω_K = real and imaginary parts of the characteristic exponent
 $\eta_i, \zeta_i, \theta_i$ = mode shapes for flap, lag, and torsion
 θ = pitch angle, rad
 λ_K = characteristic exponent
 $\bar{\lambda}$ = steady inflow (free stream plus induced flow)
 μ = advance ratio
 v = inflow parameter, Eq. (5)
 v_o, v_c, v_s = uniform, longitudinal, and lateral inflow components
 σ = solidity ratio = $bc/\pi R$
 ψ = azimuth angle, nondimensional time
 $\omega_w, \omega_v, \omega_\phi$ = nondimensional rotating flap, lag, and torsional frequencies
 Ω = blade rotational speed, rad/sec
 $(\bar{\quad})$ = nondimensionalized quantity, equilibrium deflection
 $(\dot{\quad})$ = time derivative

Introduction

Hingeless rotor blades are less complex mechanically and provide more rotor control power and damping than articulated rotor blades. However, the complex aeroelastic behavior of hingeless rotors requires a rigorous analysis for an effective design procedure. The modeling requirements of hingeless-rotor-blade aeroelasticity have been studied for many years and are briefly reviewed here.

Initial analyses focused on the investigation of flap-lag stability of torsionally rigid blades with spring-restrained hinges at the hub to simulate bending flexibility. The stability of this type of model was analyzed for both hover¹ and forward flight.² Flap-lag stability of elastic blades with uniform properties was studied by Ormiston and Hodges,¹ based on a derivation of nonlinear partial differential equations suitable for elastic hingeless blades. Similar equations were studied by Friedmann and Tong.³ Efforts were also made to investigate the complete blade problem by including blade torsional deflections. Friedmann and Tong³ approximated the torsional deflection by rigid-body pitching motion (root torsion); they found that torsion motion was important and that the stability characteristics were sensitive to the number and type of assumed bending-mode shapes used. Flap-lag structural coupling was not included. Hodges and Ormiston⁴ presented extensive numerical results for the stability characteristics of elastic hingeless blades with flap-lag-torsion motion in hover. They found that torsional deflections of hingeless rotor blades are strongly influenced by the nonlinear structural moments caused by flap and lead-lag bending. This bending-torsion structural coupling is proportional to the product of the flap and lead-lag bending curvatures and to the difference between the two bending flexibilities. This study also showed the effect of precone, structural coupling, and torsional rigidity on the isolated blade stability boundaries.

Friedmann and Kottapalli⁵ analyzed the coupled flap-lag-torsional dynamics of hingeless rotor blades in forward flight. They noted that nonlinearities are important in an aeroelastic stability analysis and that forward flight is strongly coupled with the trim state. However, only flap-ping motion was used in calculating the rotor trim condition. It was observed that forward flight (increasing advance ratio) is stabilizing for soft inplane rotors and destabilizing for stiff inplane rotors. In all these studies, the aerodynamic forces were obtained from strip

theory based on a quasi-static approximation of two-dimensional, unsteady airfoil theory.

Simultaneous efforts have been made to improve the aerodynamic model used in these analyses by including unsteady airflow effects. One approach is to model the induced velocity as a time-dependent, three-degree-of-freedom system. This dynamic inflow theory has been applied to rigid-blade flap-lag analyses, both in hover and forward flight,⁶⁻⁸ and to the coupled rotor-fuselage problem in hover.^{9,10} It was observed that the dynamic inflow increased the lag regressing-mode damping and reduced the body pitch and roll damping for the parameters considered. These analytical results correlated well with experimental results.¹⁰ However, the conclusions presented in Refs. 6-10 were based on several restrictive assumptions; for example, zero elastic coupling, fixed solidity ratio, and rigid flap-lag rotor-blade models with no torsional flexibility. The effects of dynamic inflow and torsion flexibility on the aeroelastic stability of an elastic rotor blade in hover to a number of parameters was recently presented.¹¹ It was shown that for torsionally flexible blades, the dynamic inflow effects depend on the elastic coupling parameter. For certain values of elastic coupling, the dynamic inflow effect may in fact be negligible.

In summary, general nonlinear differential equations for the elastic rotor blades (used in the above analyses) have been developed by several researchers.¹²⁻¹⁴ These models have elastic flap, lead-lag, and torsion degrees of freedom, with nonlinearities owing to moderate elastic deflections. In those studies, it was observed that for a given ordering scheme, the final equations differed by a number of small nonlinear terms. These differences depend in part on the stage at which, in the process of derivation, the ordering scheme is applied. The application of the ordering scheme at a later stage in the derivation process requires much time in deriving and independently checking the final equations. This has led to attempts to share the algebra with computers through symbolic processors. Both general and special purpose programs have been developed and are available.¹⁵ The program Helicopter Equations for Stability and Loads (HESL), appropriate to rotary-wing aeroelasticity investigations written in FORTRAN IV, was presented in Ref. 16. The approach used in developing this program and its use in analyzing the aeroelastic stability of an elastic rotor blade in hover was presented in Ref. 11.

In the present paper, the HESL program has been extended to derive the gov-

erning equations of motion for an elastic rotor blade in forward flight. A Lagrangian formulation is used to obtain the equations in generalized coordinates. The program generates the steady-state and linearized perturbation equations in symbolic form and then codes them into FORTRAN subroutines. Subsequently the coefficients for each equation and for each mode are identified through a numerical program. The harmonic balance equations, if required in the calculation of the deflected equilibrium position of the blade, can also be obtained from the symbolic program. The governing multiblade equations are derived explicitly using HESL. This is the first time that multiblade equations are derived explicitly using this symbolic formulation approach to study the stability of an elastic rotor blade in forward flight. The multiblade equations are capable of accommodating any number of elastic blade modes. Because the complete analytical process, from derivation to numerical calculation, is automated, it is an efficient and accurate means for analyzing helicopter rotor aeroelasticity.

The present study differs from previous ones in the following respects: 1) symbolic manipulation with FORTRAN is used to derive the governing equations in forward flight for an elastic rotor blade; 2) complete elastic flap-lag-torsion blade degrees of freedom are used for the trim calculation; 3) explicit multiblade equations are derived symbolically for stability calculation to compare with the single-blade solution; 4) dynamic inflow is included in the aeroelastic stability solution of an elastic blade in forward flight; and 5) damping data in forward flight are presented for varying elastic structural coupling.

To demonstrate the usefulness of this analytical capability, stability results are presented for several hingeless-rotor-blade structural models. The influence of dynamic inflow in forward flight with an elastic hingeless rotor is also investigated. The hingeless-rotor stability results presented in this paper using the symbolic program reflect the combined effect of an improved structural model (by including torsion) and an improved aerodynamic model (by including dynamic inflow). Results are presented for elastic blade flap-lag-torsion analysis and for flap-lag analysis with and without dynamic inflow.

Formulation

Figure 1 shows an elastic blade with the coordinate system used in this study. The blade has uniform mass and stiffness,

no twist, and no chordwise offsets of the elastic axis, tension axis, or center of mass. The elastic axis is coincident with the x-axis of the x,y,z coordinate system rotating with a constant angular velocity (Ω) about a fixed point at the origin. The y-axis lies in the plane of rotation, and the x-axis is rotated through a small angle (β_{pc}) from the plane of rotation. The deflections of the beam are u (axial deflection), v (lagwise bending), and w (flapwise bending) of the elastic axis parallel to the x,y,z coordinates, respectively. A second coordinate system, x', y', and z', is fixed to the blade, with y' and z' axes parallel to the principal axes of the deformed blade cross section. This coordinate system moves with the blade cross section as it undergoes bending, torsional displacements, and pitch angle (θ) rotation. Before deformation, the principal axes of the blade cross section are rotated with respect to the undeformed coordinates by the pitch angle. After deformation, the elastic axis is displaced by u,v,w, and the blade is twisted through the angle ϕ . The aerodynamic inflow dynamics couple with the blade dynamics as a feedback loop (Fig. 2). The total inflow (v_i) is assumed to consist of a steady value ($\bar{\lambda}$) and dynamic inflow components (v_0 , v_c , and v_g) that vary with time.

In this study, the entire problem formulation is performed by the computer; there is minimum user interface other than specifying blade geometry and the desired blade model representation. In general, the formulation of the rotary-wing aero-elastic problem consists of the following: writing the transformation matrices between the coordinate systems before and after deformation; calculating the position vector of a mass point of the deformed blade section; forming strain displacement relations; and calculating stresses and air velocity components in the flap, lag, and torsion directions (see Refs. 12-14 for more details). These expressions include geometrical nonlinearities owing to the assumption of small strains and moderate deflections which give rise to numerous higher-order nonlinear terms. So an ordering scheme, based on assigning orders of magnitude to the various physical parameters, is used to reduce the number of terms. The governing equations of motion are then obtained using Hamilton's principle. These equations are nonlinear, partial differential equations in u,v,w, and ϕ deflections. These are converted to ordinary differential equations using Galerkin's method by expressing the bending and torsion deflections in terms of generalized coordinates and mode-shape functions,

$$w = \sum_{i=1}^{N_F} R w_i(\psi) \eta_i(\bar{x})$$

$$v = \sum_{i=1}^{N_L} R v_i(\psi) \zeta_i(\bar{x}) \quad (1a)$$

$$\phi = \sum_{i=1}^{N_T} \phi_i(\psi) \theta_i(\bar{x})$$

and by expressing the induced velocity as

$$v_i = \bar{\lambda} + v_0 + v_c \bar{x} \cos \psi + v_g \bar{x} \sin \psi \quad (1b)$$

where $\psi = \Omega t$, $\bar{x} = x/r$, and $\eta_i, \zeta_i, \theta_i$ are mode shapes; R is the blade radius; and N_F, N_L , and N_T are the numbers of flap, lag, and torsion modes, respectively, used in the analysis. In this study uncoupled rotating modes evaluated at zero pitch are used. This yields N nonlinear, non-homogeneous ordinary differential equations in terms of modal generalized coordinates w_i, v_i , and ϕ_i , where N is the total number of flap, lag, and torsion modes used in the analysis. The equations have periodic coefficients in the mass, damping, and stiffness matrices. These equations are then linearized for small perturbation motions about the deformed blade time-dependent equilibrium position by expressing the generalized coordinates in terms of the equilibrium quantities and small perturbation quantities:

$$w_i = \bar{w}_i(\psi) + \Delta w_i(\psi)$$

$$v_i = \bar{v}_i(\psi) + \Delta v_i(\psi) \quad (2)$$

$$\phi_i = \bar{\phi}_i(\psi) + \Delta \phi_i(\psi)$$

Two sets of equations are obtained from this operation: a set of N nonlinear equations in \bar{w}_i, \bar{v}_i , and $\bar{\phi}_i$, which define the deflected equilibrium position of the blade, and a set of N equations obtained by subtracting the equilibrium equations and discarding all nonlinear products of the perturbation quantities, $\Delta w_i, \Delta v_i$, and $\Delta \phi_i$. Three more equations are obtained for the dynamic inflow components from rotor perturbations in aerodynamic thrust (C_T) and in pitch (C_M) and roll (C_L) moments (see Dynamic Inflow, below). The coefficients of these equations are also functions of the equilibrium solution.

Dynamic Inflow

The dynamic inflow equations are related to the blade degrees of freedom through the variations in thrust, pitching, and rolling moments:

$$[m] \begin{Bmatrix} \dot{v}_O \\ v_C \\ v_S \end{Bmatrix} + [l]^{-1} \begin{Bmatrix} v_O \\ v_C \\ v_S \end{Bmatrix} = \begin{Bmatrix} C_T \\ C_M \\ C_L \end{Bmatrix} \quad (3)$$

The elements of $[m]$ and $[l]$ define the various dynamic inflow models that can be included in an analysis. Reference 8 presents a hierarchy of models having different elements for $[m]$ and $[l]$ from actuator disk theory in forward flight. The elements of $[l]$ depend on the wake skew angle at the rotor:

$$\alpha_R = \tan^{-1} \left[\frac{\bar{\lambda}}{\mu} \right] \quad (4)$$

where $\bar{\lambda}$ is the steady inflow.

Of the 13 models presented in Ref. 8, the partially constrained model gave good results. In the present paper, this partially constrained theory is used to obtain the dynamic inflow results. The elements of $[m]$ and $[l]$ are given by

$$\begin{aligned} m_{11} &= \frac{128}{75\pi}, & m_{22} &= m_{33} = \frac{-16}{45\pi}, \\ m_{ij} &= 0, & i &\neq j \\ l_{11} &= \frac{1}{2}, & l_{13} &= \frac{15\pi}{64} \left(\frac{1 - \sin \alpha_R}{1 + \sin \alpha_R} \right)^{1/2}, \\ l_{22} &= \frac{-4}{1 + \sin \alpha_R} \\ l_{31} &= l_{13}, & l_{33} &= \frac{-4 \sin \alpha_R}{1 + \sin \alpha_R}, \\ l_{12} &= l_{21} = l_{23} = l_{32} = 0 \\ l_{ij} &= \frac{1}{v} l_{ij}, & v &= \frac{\mu^2 + \bar{\lambda}(2\bar{\lambda} - \mu \tan \alpha)}{(\mu^2 + \bar{\lambda}^2)^{1/2}} \end{aligned} \quad (5)$$

Equations from HESL

The governing equations of motion of the rotor blade are derived using HESL with two modes for each blade degree of freedom. The principles involved in the development of the symbolic program HESL are described in detail in Refs. 11, 16, and 17. Basi-

cally, the program assigns numbers to the variables forming the required expressions and then manipulates those numbers to obtain the required algebraic quantities. The integration, differentiation, perturbation, and multiblade coordinate transformation are performed by substituting known relations required for these operations. The symbolic program can handle both individual expressions and matrices. The program generates the steady and perturbed equations in a single operation and outputs them individually. This is convenient in the case of forward flight because of the large number of terms present in each equation; it is also convenient for the different analytical processes required for the steady and perturbed sets of equations.

The inputs to the program are the relations, in alphanumeric format, for the position vector, for the strain expressions, for the air-velocity components, and for the transformation matrices as given by Kaza and Kvaternik.¹³ The integration relations (if known), differentiation relations, the order of the variables, the ordering scheme to be used, and the variables for which coefficients are to be collected are also given as data. In the present paper, the order of the variables and the ordering scheme used are the same as those followed in Ref. 4. All the $O(\epsilon)^2$ terms, compared to $O(1)$, except those that contribute to lead-lag and torsion damping, are neglected. Nonlinear rate products ($\dot{v}\dot{w}$, \dot{v}^2 , etc.) are retained since they contribute to the linearized stability analysis. Although any general ordering scheme could have been used to obtain the final equations of motion, this ordering scheme is considered representative and adequate for demonstrating the capability of the symbolic analysis process. The program calculates the strain energy, kinetic energy, and generalized forces for a given ordering scheme in generalized coordinates using Eq. (1). The perturbation relations as given in Eq. (2) are substituted to obtain the steady and perturbed terms. The program generates both the steady-state (nonlinear) and linearized perturbation equations and the loading terms necessary for an aeroelastic stability and response analysis. The rotor-thrust, pitch-moment, and roll-moment equations required in the dynamic inflow equations are also obtained using the perturbed aerodynamic forces. The equations are written into FORTRAN sub-routines for subsequent numerical calculations. A numerical program subsequently identifies the mass, damping, stiffness, and forcing coefficients for each generalized degree of freedom. For the results presented here, it took about 300 sec to symbolically derive both the structural

and aerodynamic equations on a VAX 11/780 computer.

A brief description of the program input and output follows. Figure 3 is a flow diagram of the aeroelastic analysis using the symbolic and numerical programs. Table 1 shows the FORTRAN symbol definitions used for the original variables. Table 2 shows the input required to calculate tangential and perpendicular blade cross-section velocities U_T and U_P , using the transformation matrix $LAPP(READ MATRIX)$ and the air-velocity vector $VEL(READ MATRIX)$. By multiplying the two matrices (FORM MATRIX) with ordering scheme *E2D1, the vector $AVEL$ is obtained, which gives the components of the velocities in radial, tangential, and perpendicular directions. The vector components are redefined as expressions by command $MATRIX EXPRESSION$. The actual velocity components are the negative of the original expression, and are therefore negated by calling the $NEGATE$ command, thus giving the actual velocity expressions. This procedure is slightly different from the one presented in Ref. 11, where manipulations were performed at the expression level. Here the manipulations are extended to include matrix operations. It should be noted that for a hingeless rotor, the axial displacement can be solved for a priori as a function of flap and lag bending. In the present paper, expressions for axial displacement and axial velocity are taken from Ref. 4 and supplied as data to the program.

Trim and Periodic Equilibrium Solution

The nonlinear periodic coefficient equations obtained earlier can be solved for the periodic response in the time domain using a Floquet method or in the frequency domain using a harmonic balance method. Either will yield the time-dependent equilibrium position about which the nonlinear equations can be linearized for an eigensolution. In forward flight, this equilibrium position is coupled with the entire trim state of the helicopter. The trim state is the steady-state condition achieved by the system as time increases without bound, with the controls fixed and no external output. Calculation of trim position requires establishing the control settings for a given flight condition. The control settings are collective pitch, longitudinal and lateral cyclic pitch, and the rotor-shaft angle of attack. The induced velocity, which depends on the generated thrust and advance ratio, is also calculated.

In this paper, the harmonic analysis method, coupled with an iteration on the trim state, is used to calculate the equilibrium position and the trim settings.

This procedure¹⁰ consists of the following. An iterative inner loop in which the solution for the periodic motion is obtained with fixed values of the trim variables is nested within an outer loop in which the solution for the trim variables is obtained. The rotorcraft motion is solved for the periodic motion by the harmonic analysis method, which directly calculates the harmonics of a Fourier series representation of the motion. The procedure advances the rotor around the azimuth, calculating the forcing functions in the time domain and then updating the harmonics of the response. The forces and moments acting on the rotor are calculated from this response and the controls are adjusted until the equilibrium of forces and moments required for the specified operating state is achieved.

For the harmonic analysis method, the governing equations of motion are written, with all the time-dependent and nonlinear terms as a forcing function, as

$$[M]\{\ddot{X}\} + [C]\{\dot{X}\} + [K]\{X\} = F(\dot{X}, X, \psi) \quad (6)$$

where matrices M , C , and K are the constant mass, damping, and stiffness matrices and X is the vector of degrees of freedom. The function F is evaluated at J points around the rotor azimuth

$$F_j = F(\psi_j) \quad (7)$$

and the harmonics of a complex Fourier series representation of F are given by

$$F_n = \frac{1}{J} \sum_{j=1}^J F_j e^{-in\psi_j} \quad (8)$$

Then the n th harmonic of the motion is given by

$$X_n = H_n^{-1} F_n \quad (9)$$

where

$$H = K - n^2 M + iCn$$

The iterative solution proceeds as follows. At a given azimuth ψ_j , the blade motion is calculated using the current estimates of the harmonics:

$$X = \sum_{n=-L}^L X_n e^{in\psi_j} \quad (10)$$

$$\dot{X} = \sum_{n=-L}^L X_n in e^{in\psi_j}$$

where L is the number of terms used in the complex expansion of X . The forcing

function is evaluated with this motion. Then the change in the harmonics owing to the change in the forcing function is calculated and added to the harmonics calculated in the last revolution. After every revolution, the old and new harmonics are checked until convergence.

After obtaining the harmonics of the blade motion, the equilibrium of the forces and moments is checked. If equilibrium is not satisfied, the trim settings are increased and the procedure is repeated until equilibrium is met. The following assumptions are made in arriving at the equilibrium of the forces and moments. The helicopter is in straight and level steady flight; the rotor-hub moments are trimmed to zero; and tail, fuselage moments, and side-force components are neglected. Then the equilibrium forces and moments are given by

$$\begin{aligned} \bar{C}_T \cos \alpha + C_H \sin \alpha &= C_w \\ -\bar{C}_T \sin \alpha + C_H \cos \alpha &= -C_x \quad (11) \\ C_{mx} &= C_{my} = 0.0 \end{aligned}$$

where $C_x = (1/2)\bar{\Gamma}\mu^2$ and α is the angle of attack of the shaft.

In calculating thrust, horizontal force, and the hub moments, the steady inflow appears as a parameter that in turn depends on the rotor thrust and shaft angle of attack. In this paper, the steady inflow is taken as an equation of constraint and solved along with the four equations above:

$$\bar{\lambda} - \mu \tan \alpha - \bar{C}_T / [2(\bar{\lambda}^2 + \mu^2)^{1/2}] = 0.0 \quad (12)$$

The increments in the trim settings are calculated using a modified Newton-Raphson method.¹⁸ If v is the control variable and M is the target to be achieved, then a first-order approximation of $M(v)$ is

$$M(\text{target}) = M_{n+1} = M_n + \frac{\partial M}{\partial v} (v_{n+1} - v_n) \quad (13)$$

or

$$v_{n+1} = v_n + D^{-1} [M(\text{target}) - M_n] F$$

where v_n and v_{n+1} indicate the current and new estimates of v , respectively, and $F < 1$ is included to avoid overshoot oscillations in the trim iteration by reducing the step size. The partial derivative matrix D is

$$\begin{aligned} D = \frac{\partial M}{\partial v} &= \left[\dots \frac{\partial M}{\partial v_i} \dots \right] \\ &= \left[\dots \frac{M(v_i) - M(v_i - \Delta v_i)}{\Delta v_i} \dots \right] \quad (14) \end{aligned}$$

where v_i is the i th control variable and Δv_i is its increment. The convergence is checked when the tolerance level, as specified by the parameter ϵ , is met. For more details on this procedure see Ref. 18. In the present paper, all the degrees of freedom—blade flap, lead-lag, and torsion degrees of freedom—are used in calculating the trim state and periodic response.

The periodic response can also be obtained using Floquet methods.³ A review of the use of these methods to obtain the initial conditions, forced response, and stability data is given in Ref. 19.

Aeroelastic Stability Solution: Single Blade

Once the time-dependent equilibrium position is determined, the nonlinear equations are perturbed about this equilibrium position, as given by Eq. (2). As mentioned earlier, the symbolic program generates the perturbed equations and writes them into subroutines. It should be noted that squares of the perturbation quantities are neglected by the symbolic program by employing the ordering scheme. The final system of equations for stability is

$$[P]\{\Delta \ddot{q}\} + [Q]\{\Delta \dot{q}\} + [R]\{\Delta q\} = 0 \quad (15)$$

or

$$\{\dot{z}\} = [A_S]\{z\}$$

The stability of this linearized system is determined from Floquet theory by evaluating the characteristic exponents of $[A_S]$,

$$\lambda_K = \zeta_K + i\omega_K \quad (16)$$

The mass, damping, and stiffness terms are identified by a numerical program for each time-step. The linearized system is stable when $\zeta_K < 0$.

Multiblade Coordinate Transformation

To provide a better understanding and to include dynamic inflow effects, which are referenced to the fixed system, it is necessary to convert the equations into a fixed coordinate system. In the case of

hovering flight, this transformation can be easily performed by rearranging the coefficients of the equations, since the coefficients are constant. For forward flight, the degrees of freedom, as well as the coefficients, are periodic. Hence, the multiblade coordinate transformation (MCT) is more complicated. The MCT or Fourier coordinate transformation is a linear transformation of the degrees of freedom from the rotating to nonrotating frame. Let X be a degree of freedom (dimensionless) in the rotating frame for the i th blade. Then, for a three-bladed rotor, the relations

$$\begin{aligned} X_i &= X_0 + X_C \cos \psi_i + X_S \sin \psi_i \\ \dot{X}_i &= \dot{X}_0 + (\dot{X}_C + X_S) \cos \psi_i + (\dot{X}_S - X_C) \sin \psi_i \\ \ddot{X}_i &= \ddot{X}_0 + (\ddot{X}_C + 2\dot{X}_S - X_C) \cos \psi_i \\ &\quad + (\ddot{X}_S - 2\dot{X}_C - X_C) \sin \psi_i \end{aligned} \quad (17)$$

give the i th blade degree of freedom, using multiblade coordinates in the nonrotating frame. The variables X_0 , X_C , and X_S are the rotor degrees of freedom, and describe the motion of the rotor as a whole in the nonrotating frame.

The MCT involves the following steps²⁰: 1) expansion of each degree of freedom into multiblade coordinates; 2) multiplying the resulting expression with multiblade functions like 1, $\cos \psi$, $\sin \psi$, $\cos 2\psi$, $\sin 2\psi$, etc., depending on the number of blades; 3) replacing products of sines and cosines as sums of sines and cosines, using trigonometric relations; and 4) deleting terms that are not multiples of the number of blades (summation rules). Using the symbolic program, this is achieved as follows. The multiblade expansions of each degree of freedom and their time derivatives are given as a table of relations (Eq. (17)). The multiblade functions like 1, $\cos \psi$, $\sin \psi$, $\cos 2\psi$, $\sin 2\psi$, etc., required in transforming the equations, are read as data (or can be generated within the program). The trigonometric relations giving the product of sines and cosines as sums of sines and cosines are given as a table of relations. These require that the equation derivation be several runs until all the required relations are included in the table of relations. Then the command PERFORM MULTIBLADE TRANSFORMATION multiplies the equation with each of the multiblade functions, substitutes the multiblade expansion for each degree of freedom, substitutes the trigonometric relations (from the given tables of relations), and checks for the multiples of the blade harmonics. Only terms containing multiples of the number of blades are retained. The interface routines separate the terms into constant and periodic

parts, with the coefficient of each harmonic separated, and writes them into subroutines. In this manner, the constant-coefficient approximation is easily done. In the present paper, the perturbed governing equations of motion and perturbations in thrust and moment equations are converted into multiblade coordinates. The multiblade solution was checked for accuracy with a single-blade solution without dynamic inflow. It should be noted that the trim-value harmonics entering as nonlinear contributions should be defined as symbolic data. The input data increase as more nonlinear terms are taken into account in addition to the data given for the multiblade expansion of the degrees of freedom. However, the output may be smaller since only terms that are multiples of the number of blades are retained. Since this is a feasibility study undertaken to obtain explicit multiblade equations using a symbolic program in FORTRAN, the nonlinear quantities are assumed to provide only first harmonic forcing contributions. For the results presented here, the program was run on a VAX 11/780 computer. It took about 250 sec to derive the multiblade equations for each blade degree of freedom, and about 120 sec to write these into subroutines for numerical analysis.

It should be noted that by giving the expansion of each degree of freedom into its harmonics and by giving the trigonometric relations as data to the symbolic program, explicit harmonic balance equations can also be derived. However, because of the amount of input required to perform a symbolic formulation of the harmonic balance and multiblade equations, the program HESL is convenient for explicitly considering the symbolically derived equations only if the number of degrees of freedom is small. As pointed out in Ref. 20, numerical schemes are better suited to general models for efficiently obtaining the harmonic balance equations and multiblade equations after the steady and perturbed equations are obtained from the symbolic program.

The symbolic program separates the terms containing the periodic variable $\cos Nt$ and $\sin Nt$ and writes the equation as

$$A(t) = A_0 + A_N \cos Nt + B_N \sin Nt \quad (18)$$

In subroutine form they are referred to as A(1), A(2), and A(3). This allows for direct elimination of the matrices A(2) and A(3) for a simple constant-coefficient approximation analysis.

Stability Solution: Multiblade and Dynamic Inflow

The final governing equations of motion can be written as

$$[P]\{\ddot{q}\} + [Q]\{\dot{q}\} + [R]\{q\} + [T]\{u\} = 0 \quad (19a)$$

for the blade equations, and as

$$[A]\{\ddot{q}\} + [B]\{\dot{q}\} + [C]\{q\} + [G]\{u\} = [m]\{\ddot{u}\} + [l]^{-1}\{u\} \quad (19b)$$

for the dynamic inflow equations, where

$\{q\}$ is $\{q_c, q_{c'}, q_g\}$

$\{q_c\}$ is vector of all collective modes

$\{q_{c'}\}$ is vector of all lateral cyclic modes

$\{q_g\}$ is vector of all longitudinal cyclic modes

$\{u\}$ is $\{v_o, v_{c'}, v_g\}$

Defining $\dot{\Lambda} = \{u\}$, Eqs. (19a) and (19b) can be combined as

$$\begin{bmatrix} P & 0 \\ A & -m \end{bmatrix} \{\ddot{X}\} + \begin{bmatrix} Q & T \\ B & (G - l^{-1}) \end{bmatrix} \{\dot{X}\} + \begin{bmatrix} R & 0 \\ C & 0 \end{bmatrix} \{X\} = 0 \quad (20)$$

where $\{X\}$ is

$$\begin{Bmatrix} q \\ \Lambda \end{Bmatrix}$$

The final stability equations in state vector form are

$$\{\dot{Y}\} = [A_g]\{Y\} \quad (21)$$

where

$$\{Y\} = \begin{Bmatrix} X \\ \dot{X} \end{Bmatrix}$$

The stability results are obtained by calculating the eigenvalues of $[A_g]$, in a manner similar to that used in the single-blade case.

The size of the state matrix depends on the number of modes and blades. For the flap-lag-torsion model with two modes each, the size of the state matrix is 36×36 without dynamic inflow and 39×39 with dynamic inflow. The corresponding values

for a flap-lag model are 24×24 and 27×27 , respectively.

Results and Discussion

Results are presented for a uniform blade with zero built-in twist, zero precone angle and zero blade offsets. Reversed-flow effects are neglected. A three-bladed rotor is considered. Two rotating modes for each flap, lag, and torsion degrees of freedom are used in the calculation. These modes are calculated at zero pitch and are obtained from five nonrotating modes. Results for both a single-blade solution and a multiblade solution are presented for different blade structural models. All results are for a propulsive trim condition, specified for a weight coefficient of $C_W/\sigma = 0.07$ and an equivalent drag area $D/q = f = 0.001(\pi R^2)$, where D is the drag force, and q is the dynamic pressure.

In the derivation of the equations, the order of magnitude assigned for each parameter is the same as that followed in Ref. 4. The other parameters used for the numerical study are

$$\begin{aligned} \omega_v &= 0.7, 1.4; \omega_w = 1.15; \omega_\phi = 3.0; \\ c/R &= 0.07854; \gamma = 5.0; \sigma = 0.1; \\ a &= 2\pi; C_{d0} = 0.01; \beta_{pc} = 0.0; \\ K_{m1}/K_{m2} &= 0.0; K_m/R = 0.025; \\ (K_A/K_m)^2 &= 1.5 \end{aligned}$$

Lead-lag damping values (real part of the characteristic exponent) are presented for a soft inplane and a stiff inplane rotor with and without dynamic inflow. The results are presented for investigating 1) the effect of degrees of freedom used in the trim analysis on the lead-lag damping, 2) the effect of using only one torsion mode, 3) the inclusion of a dynamic inflow model, and 4) the difference between periodic and a constant-coefficient approximation.

Single-Blade Results

The effect of the number of degrees of freedom used in the trim analysis on the lead-lag damping is shown in Figs. 4 and 5. Figure 4 shows the lead-lag damping plotted versus advance ratio for a soft inplane rotor ($\omega_v = 0.7$). It can be seen that a flap-lag-torsion stability analysis from a flap-trim analysis underpredicts the lead-lag damping. The second mode shows the same trend with the difference in predicted damping increasing with advance ratio. Figure 5 shows the lead-lag damping plotted for a stiff inplane

rotor ($\omega_v = 1.4$) as a function of advance ratio. The results also show an increase in damping when a flap-lag-torsion trim analysis is used. It is also noted that for an advance ratio of $0.37 < \mu < 0.41$, the first-mode roots separate and one root becomes less stable and the other becomes more stable. The damping does reduce as the advance ratio is increased. The second mode remains stable at all advance ratios considered.

The increase in damping observed above for both soft inplane and stiff inplane rotors is perhaps a result of the different time-dependent equilibrium positions used. A full flap-lag-torsion trim analysis is consistent in that the blade model has the same degree of complexity in both the trim and the stability analysis. It should be noted that qualitatively the same type of trend was reported in Ref. 5, for both soft inplane and stiff inplane rotors. This verifies the symbolic and numerical programs for the single-blade results and forms the basis for checking the symbolically derived multiblade equations (and numerical results) subsequently.

Figures 6 and 7 present the lead-lag damping plotted versus advance ratio from a flap-lag model, flap-lag-torsion model (two modes for each degree of freedom), and flap-lag-torsion model with only one torsion mode, for a soft inplane rotor ($\omega_v = 0.7$). Figure 6 presents the damping results for full elastic coupling ($R = 1.0$). It can be seen that the flap-lag model underpredicts the lead-lag damping. The model with only one torsion mode increases the damping above that of the model with two modes each. Figure 7 shows the lead-lag damping value plotted for zero elastic coupling ($R = 0.0$). The damping levels are very much reduced compared with those in the full elastic coupling case. However, the flap-lag model is again the least damped.

Lead-lag damping is plotted for a stiff inplane rotor ($\omega_v = 1.4$) with varying advance ratio in Figs. 8 and 9. Figure 8 presents the damping results for full elastic coupling. The same trend that was observed for the case of soft inplane (Fig. 6) exists. Here, it is to be noted that root splitting for high advance ratios occurs even when only one torsion mode is used. Figure 9 presents the lead-lag damping for increasing advance ratio for a stiff inplane rotor for zero elastic coupling parameter. Although a flap-lag model predicts a stable system, the rotor is unstable. This demonstrates the importance of elastic blade torsion in a forward-flight stability analysis.

Figure 10 shows the lead-lag damping plotted for an advance ratio of $\mu = 0.25$

while varying the elastic coupling parameter for a stiff inplane rotor. Here a flap-lag model predicts positive damping for all values of R , whereas for a flap-lag-torsion model the damping varies with the elastic coupling value, increasing with the elastic coupling parameter.

Multiblade-Equation Results

The following figures present the lead-lag regressing mode damping results obtained from multiblade equations. The multiblade equations were explicitly derived using the symbolic program. This required explicit definition of all nonlinear contributions and degrees of freedom in terms of their harmonics. The result was a significant increase in the amount of data required by the symbolic program. Since this is a feasibility study on the use of symbolic programs in FORTRAN, only first harmonics were considered in the nonlinear contributions. Consequently, damping data determined from the multiblade equations may differ from the single-blade solution. Additionally, the multiblade results are obtained by retaining only one torsion mode, although the nonlinear contribution from both torsion modes is used. This significantly reduces the time required for the Floquet stability analysis.

The damping values were first checked with those obtained from a single-blade solution obtained previously to validate the multiblade equation derivation process. It was found that the approximation $\cos \theta = 1.0$, used in deriving the explicit multiblade equations, will predict slightly higher (but less than 2%) damping for stiff inplane rotors with full elastic coupling parameter; this is because the approximation has its greatest effect on the coupling elements. For all other values of the elastic coupling parameter, this approximation does not affect the resultant damping values. Where required for comparisons, the single-blade damping values are recalculated using this approximation; this is done to avoid the rederivation of the multiblade equations.

Figures 11 and 12 show the lead-lag regressing mode damping plotted for a varying advance ratio with and without dynamic inflow from a flap-lag-torsion and flap-lag model for a soft inplane rotor. Figure 11 shows the damping for full elastic coupling ($R = 1.0$). For the flap-lag-torsion model, the dynamic inflow reduces the damping at practically all advance ratios. Its effect is negligible at advance ratios of 0.15 to 0.25. For the flap-lag model, the dynamic inflow increased the damping up to an advance ratio of 0.33; at higher advance ratios it reduced the damping. Figure 12 presents

the damping results for the zero elastic coupling ($R = 0.0$). It is seen that for the flap-lag-torsion model, the dynamic inflow again reduced the damping in hover. Yet at intermediate advance ratios, dynamic inflow increased the damping, and at higher advance ratios, it once again reduced the damping. For the flap-lag model, the dynamic inflow increased lead-lag damping for all advance ratios. This is consistent with the flap-lag model results of previous studies (e.g., Ref. 7).

The lead-lag regressing mode damping is plotted for a stiff inplane rotor for a varying advance ratio in Figs. 13 and 14. Figure 13 is for a rotor with full elastic coupling. For a flap-lag-torsion model, the dynamic inflow reduced the damping up to an advance ratio μ of 0.41. For $\mu > 0.41$, this model slowed a slightly increased damping value. The flap-lag model with dynamic inflow shows a small increase in damping. This damping increment gets smaller with higher advance ratios. Figure 14 is for a rotor with zero elastic coupling. For this configuration, the dynamic inflow increases damping for all advance ratios. Consequently both the flap-lag-torsion and flap-lag model show the same trend.

Figure 15 shows the lead-lag regressing mode damping plotted for a stiff inplane rotor at an advance ratio of 0.25, for varying elastic coupling. For the flap-lag-torsion model, dynamic inflow reduces the damping for $R > 0.3$, but it increases the available damping for $R < 0.3$. However, this increase is not sufficient to stabilize the inplane mode. With the flap-lag model, dynamic inflow shows an increase in damping for all values of elastic coupling. This is the same trend as was observed in Ref. 11 for the case of hover with both flap-lag and flap-lag-torsion blade models.

Constant-Coefficient Approximation Results

The effect of a constant-coefficient approximation (CCA) is presented in Fig. 16, where the real part of the exponent is plotted for a stiff inplane rotor with full elastic coupling that did show a splitting of roots with a full periodic coefficient analysis (Fig. 13). The CCA does not show this splitting, since the frequencies are very much away from the real axis. For this analysis, the regressing and collective modes did predict the same damping trend with advance ratio as shown by the full Floquet analysis. However, the regressing mode showed poor agreement between a CCA analysis and a Floquet-theory analysis. This is because the constant-coefficient approximation will only be good for low-frequency modes.

Conclusions

A symbolic manipulation program written in FORTRAN was used to derive the aeroelastic analysis equations of an elastic blade with flap-lag-torsion degrees of freedom in forward flight. The feasibility of using the program to obtain explicit equations in a harmonic balance method and multiblade equations was studied. Numerical results were presented, with and without dynamic inflow for a propulsive trimmed rotor. Both a flap-lag-torsion model and a flap-lag model were analyzed. Soft inplane and stiff inplane rotors were considered.

The following conclusions were drawn from this study of the use of a symbolic program for predicting rotor aeroelastic stability.

1) The symbolic program can be used to obtain explicit equations.

2) With the present program capability, the amount of data to the symbolic program increases greatly with the number of harmonics and degrees of freedom.

3) In deriving the explicit harmonic balance equations and multiblade equations, the following should be noted: a) to obtain the harmonic balance equations, a numerical method is suggested since an arbitrary number of harmonics can be used without increasing the input data to the symbolic program; b) to obtain the multiblade equations, the perturbed equations in their Fourier series form are derived using the symbolic program. Then the multiblade equations themselves are obtained numerically.

It is recommended that a selective (judicious) combination of symbolic and numerical programs is required for an efficient derivation and numerical-study process.

The following conclusions were drawn from the numerical study of a single-blade solution.

1) A flap-lag-torsion stability analysis from a trim procedure in which only the flap degree of freedom is used underpredicts the lead-lag damping.

2) In the case of stiff inplane rotors, high forward flight speed is destabilizing. At high advance ratios, a splitting of the roots is encountered, yielding two real-part characteristic exponents at the same frequency.

3) Using only one torsion mode usually increases the damping value from the flap-lag structural model.

4) The damping values for a stiff inplane rotor are very sensitive to elastic coupling parameter. Depending on this parameter, the rotor can be either stable or unstable.

The following conclusions were drawn from the numerical study of a multiblade solution with dynamic inflow.

1) For a flap-lag model, and for both soft inplane and stiff inplane rotors with zero elastic coupling, the dynamic inflow increased damping at all advance ratios considered; with full elastic coupling, the dynamic inflow increased the damping at low advance ratios, but reduced damping at high advance ratios.

2) For a flap-lag-torsion model, dynamic inflow slightly reduced lead-lag regressing-mode damping for full elastic coupling. The same trend was observed for both soft inplane and stiff inplane rotors.

3) For a given advance ratio, the variation of damping with elastic coupling parameter for a stiff inplane rotor showed the same trend as did the hover case.

4) The constant-coefficient approximation for the stiff inplane rotor does not show the splitting of the roots, since the frequency of the lag mode is away from the real axis.

References

1. Ormiston, R. A. and Hodges, D. H., "Linear Flap-Lag Dynamics of Hingeless Rotor Blades in Hover," Journal of the American Helicopter Society, Vol. 17, No. 2, 1972, pp. 2-14.
2. Peters, D. A., "Flap-Lag Stability of Helicopter Rotor Blades in Forward Flight," Journal of the American Helicopter Society, Oct. 1975, pp. 2-13.
3. Friedmann, P. P. and Tong, P., "Non-linear Flap-Lag Dynamics of Hingeless Helicopter Blades in Hover and Forward Flight," Journal of Sound and Vibration, Vol. 30, No. 1, 1973, pp. 9-31.
4. Hodges, D. H. and Ormiston, R. A., "Stability of Elastic Bending and Torsion of Uniform Cantilever Rotor Blades in Hover with Variable Structural Coupling," NASA TN D-8192, 1976.
5. Friedmann, P. P. and Kottapalli, S. B. R., "Coupled Flap-Lag-Torsional Dynamics of Hingeless Rotor Blades in Forward Flight," Journal of the American Helicopter Society, Vol. 27, No. 4, Oct. 1982, pp. 28-36.
6. Peters, D. A. and Gaonkar, G. H., "Theoretical Flap-Lag Damping with Various Inflow Models," Journal of the American Helicopter Society, Vol. 25, No. 3, 1980, pp. 29-36.
7. Gaonkar, G. H. and Peters, D. A., "Use of Multiblade Coordinates for Helicopter Flap-Lag Stability with Dynamic Inflow," Journal of Aircraft, Vol. 17, No. 2, 1980, pp. 112-118.
8. Gaonkar, G. H., Sastry, V. V. S. S., Reddy, T. S. R., Nagabhusanam, J., and Peters, D. A., "The Use of Actuator-Disk Dynamic Inflow for Helicopter Flap-Lag Stability," Journal of the American Helicopter Society, Vol. 28, No. 3, 1983, pp. 79-88.
9. Gaonkar, G. H., Mitra, A. K., Reddy, T. S. R., and Peters, D. A., "Sensitivity of Helicopter Aero-mechanical Stability to Dynamic Inflow," Vertica, Vol. 6, No. 1, 1982, pp. 57-59.
10. Johnson, W., "Influence of Unsteady Aerodynamics on Hingeless Rotor Ground Resonance," Journal of Aircraft, Vol. 19, No. 8, Aug. 1982, pp. 668-673.
11. Reddy, T. S. R., "Flap-Lag Damping of an Elastic Rotor Blade with Torsion and Dynamic Inflow in Hover from Symbolically Generated Equations," AIAA Paper 84-0989, Palm Springs, Calif., 1984.
12. Hodges, D. H. and Dowell, E. H., "Non-linear Equations of Motions for the Elastic Bending and Torsion of Twisted Nonuniform Rotor Blades," NASA TN D-7818, 1974.
13. Kaza, K. R. and Kvaternik, R. G., "Nonlinear Aeroelastic Equations for Combined Flapwise Bending, Chordwise Bending, Torsion, and Extension of Twisted Nonuniform Rotor Blades in Forward Flight," NASA TM-74059, 1977.

14. Rosen, A. and Friedmann, P. F., "Non-linear Equations of Equilibrium for Elastic Helicopter or Wind Turbine Blades Undergoing Moderate Deformation," Report No. 7718, U. of California, Los Angeles, Calif., Jan. 1977.
15. "Proceedings of the 1977 MACSYMA User's Conference," NASA CP-2012, 1977.
16. Nagabhushanam, J., Gaonkar, G. H., and Reddy, T. S. R., "Automatic Generation of Equations for Rotor-Body Systems with Dynamic Inflow for A Priori Ordering Schemes," Paper No. 37, 7th European Rotorcraft Forum, Garmisch-Partenkirchen, W. Germany, 1981.
17. Reddy, T. S. R., "Symbolic Generation of Elastic Rotor Blade Equations Using a Fortran Processor and Numerical Study on Dynamic Inflow Effects on the Stability of Helicopter Rotors," NASA TM in preparation, 1985.
18. Johnson, W., "A Comprehensive Analytical Model of Rotorcraft Aerodynamics and Dynamics. Pt. I. Analysis Development," NASA TM-81182, 1980.
19. Dugundji, J. and Wendell, J. H., "Some Analysis Methods for Rotating Systems with Periodic Coefficients," *AIAA Journal*, Vol. 21, No. 6, June 1983, pp. 890-897.
20. Johnson, W., Helicopter Theory, Princeton University Press, Princeton, N. J., 1980.

Table 1. FORTRAN symbols

| Original variable | FORTTRAN symbol | Original variable | FORTTRAN symbol |
|-------------------|-----------------|-------------------|-----------------|
| R | RAD | v' | VS |
| u | U | \bar{v}_i | LAMB |
| \dot{u} | UD | w _i | W |
| U_T | UT | w' | WS |
| U_P | UP | \dot{w} | WD |
| U_F | UF | x | XCOR |
| $U_{F'}^*$ | UFD | θ | THTA |
| v | V | ϕ | PHI |
| \dot{v} | VD | Ω | OMEG |

Table 2. Typical input to HESL and output to calculate tangential and normal velocities (U_T and U_P)

| | | | | | |
|-------------|------------|----|--|------|----------------------|
| READ MATRIX | | | | 02 | |
| #LAPP0303 | | | | -1.0 | PHI THTA |
| 03 | | | | 1.0 | %EFUR |
| 1.0 | | | | | READ MATRIX |
| -0.5 | VS | VS | | | #VEL0301 |
| -0.5 | WS | WS | | 04 | |
| 01 | | | | -1.0 | UD |
| 1.0 | VS | | | 1.0 | UFD |
| 01 | | | | 1.0 | OMEG V |
| 1.0 | WS | | | 1.0 | MU OMEG RAD CSCY |
| 02 | | | | 03 | |
| -1.0 | VS%EONE | | | -1.0 | VD |
| -1.0 | WS%ETWO | | | -1.0 | %XUUF OMEG |
| 03 | | | | -1.0 | MU OMEG RAD SNCY |
| 1.0 | %ETRE | | | 02 | |
| -1.0 | PHI THTA | | | -1.0 | OMEG RAD%LAMD |
| -1.0 | VS WS THTA | | | -1.0 | WD |
| 02 | | | | | FORM MATRIX |
| 1.0 | PHI | | | | #LAPP# VEL#AVEL*E2D1 |
| 1.0 | %EFUR THTA | | | | MATRIX EXPRESSION |
| 02 | | | | | 02#AVEL |
| 1.0 | VS%ETWO | | | | % UT0201% UP0301 |
| -1.0 | WS%EONE | | | | NEGATE EXPRESSION |
| 03 | | | | | % UT |
| -1.0 | %ETRE THTA | | | | NEGATE EXPRESSION |
| -1.0 | PHI | | | | % UP |
| -1.0 | VS WS | | | | |

Note: %EONE, %ETWO etc. are expressions read earlier in the program.

Output of U_T

```

*****
*   DETAILS OF THE EXPRESSION   UT   *
*   NUMBER OF TERMS           22   *
*****
1   1.000* VS*OMEG*  V*
2   1.000* VS*OMEG*  MU* RAD*CSCY*
3   1.000*THTA*  WS*OMEG*  MU* RAD*CSCY*
4   1.000* PHI*  WS*OMEG*  MU* RAD*CSCY*
5   1.000*  VD*
6   1.000*XCOR*OMEG*
7   1.000*  U*OMEG*
8   -1.000* UF*OMEG*
9   1.000*OMEG*  MU* RAD*SNCY*
10  -0.500* VS*  VS*  VD*
11  -0.500* VS*  VS*XCOR*OMEG*
12  -0.500* VS*  VS*OMEG*  MU* RAD*SNCY*
13  -0.500* PHI* PHI*  VD*
14  -0.500* PHI* PHI*XCOR*OMEG*
15  -0.500* PHI* PHI*OMEG*  MU* RAD*SNCY*
16  -1.000* PHI*THTA*  VD*
17  -1.000* PHI*THTA*XCOR*OMEG*
18  -1.000* PHI*THTA*OMEG*  MU* RAD*SNCY*
19  1.000* PHI*LAMB*OMEG*  RAD*
20  1.000* PHI*  WD*
21  1.000*THTA*LAMB*OMEG*  RAD*
22  1.000*THTA*  WD*

```

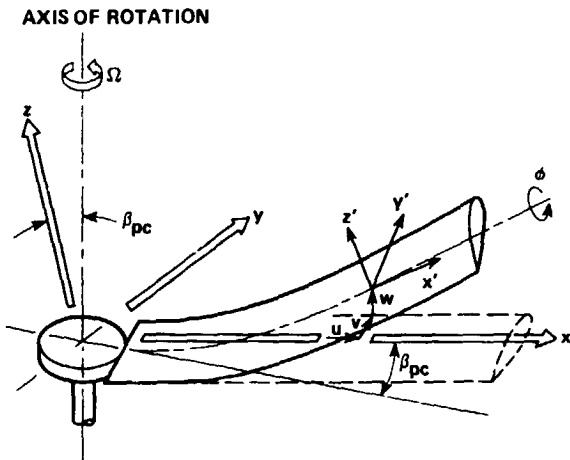


Fig. 1 Rotor-blade coordinate systems and deflections.

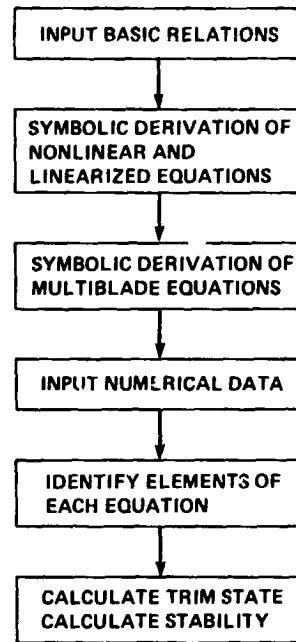


Fig. 3 Flowchart of the aeroelastic analysis.

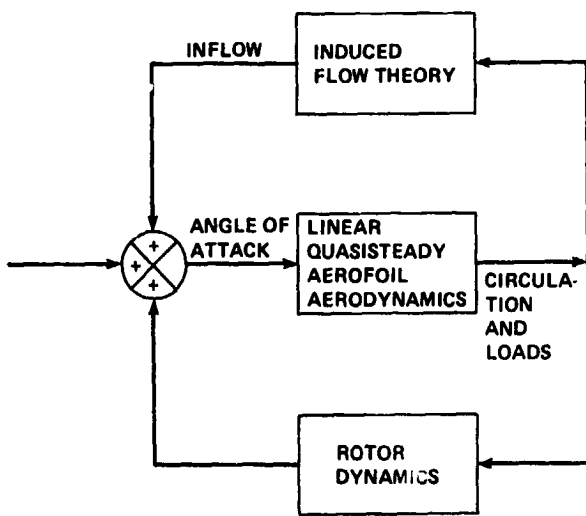


Fig. 2 Inflow dynamics.

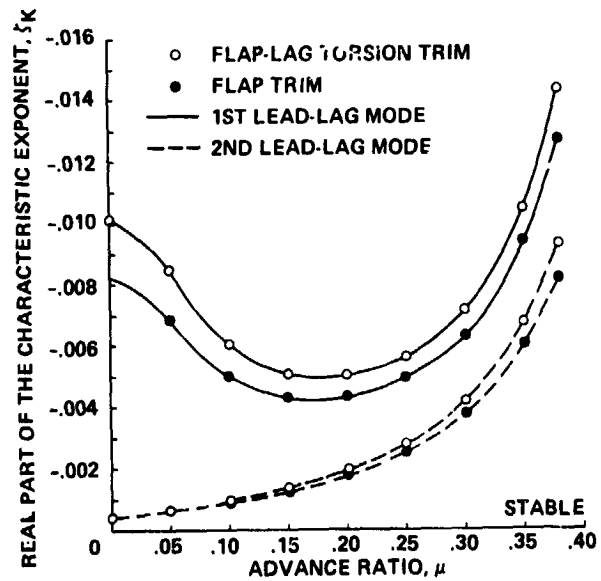


Fig. 4 The effect of the number of degrees of freedom used in trim analysis on lead-lag damping versus advance ratio: soft inplane, $\omega_v = 0.7$, $R = 1.0$, propulsive trim.

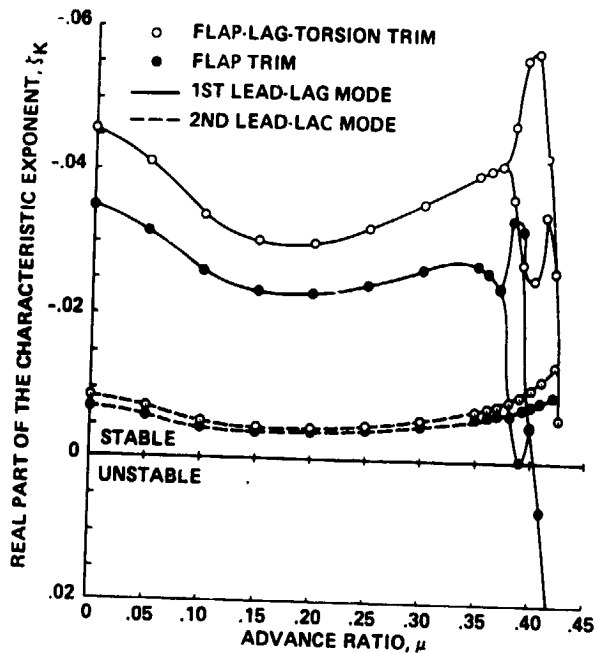


Fig. 5 The effect of number of degrees of freedom used in trim analysis on lead-lag damping versus advance ratio: stiff inplane, $\omega_V = 1.4$, $R = 1.0$, propulsive trim.

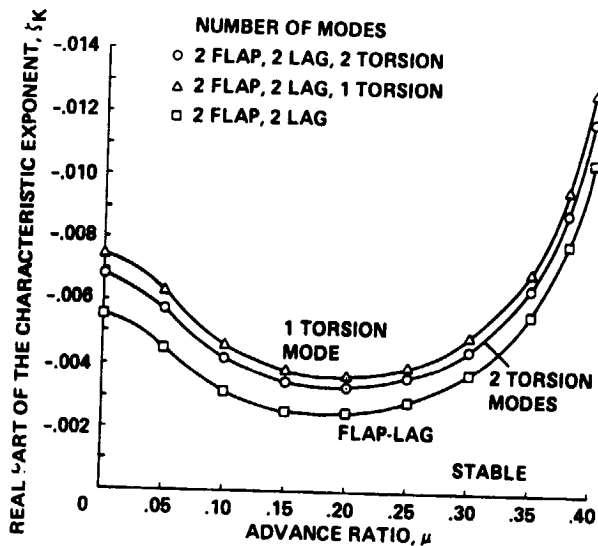


Fig. 7 Lead-lag mode damping versus advance ratio for a flap-lag-torsion model and a flap-lag model: soft inplane, $\omega_V = 0.7$, $R = 0.0$.

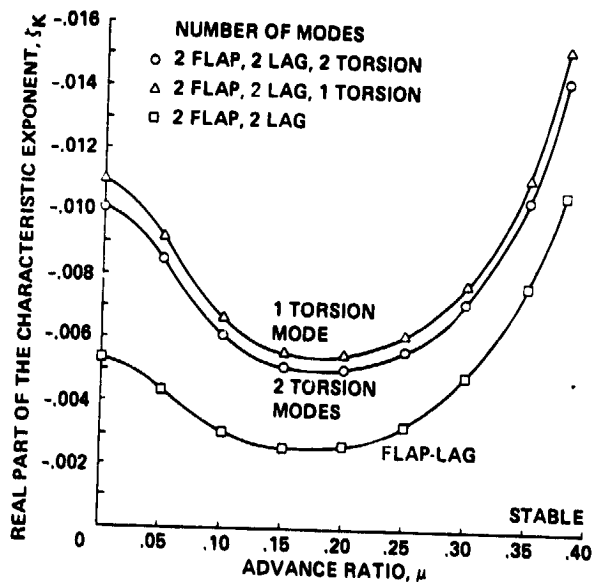


Fig. 6 Lead-lag mode damping versus advance ratio for a flap-lag-torsion model and a flap-lag model: soft inplane, $\omega_V = 0.7$, $R = 1.0$.

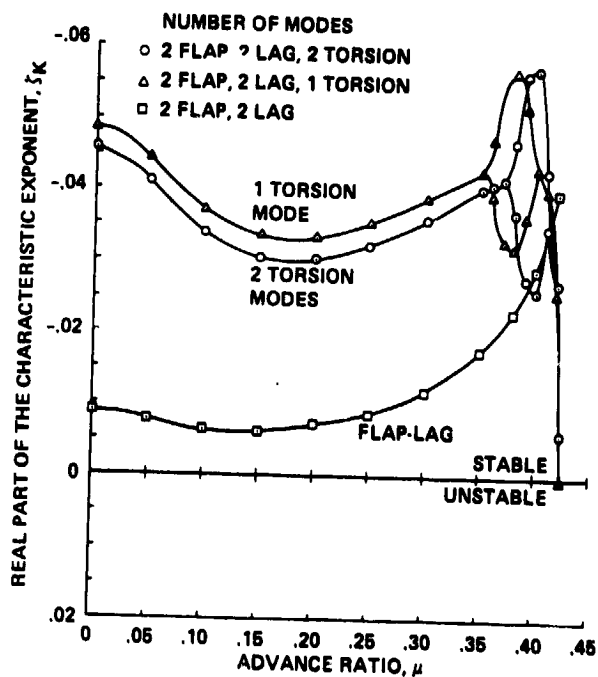


Fig. 8 Lead-lag mode damping versus advance ratio for a flap-lag-torsion model and a flap-lag model: stiff inplane, $\omega_V = 1.4$, $R = 1.0$.

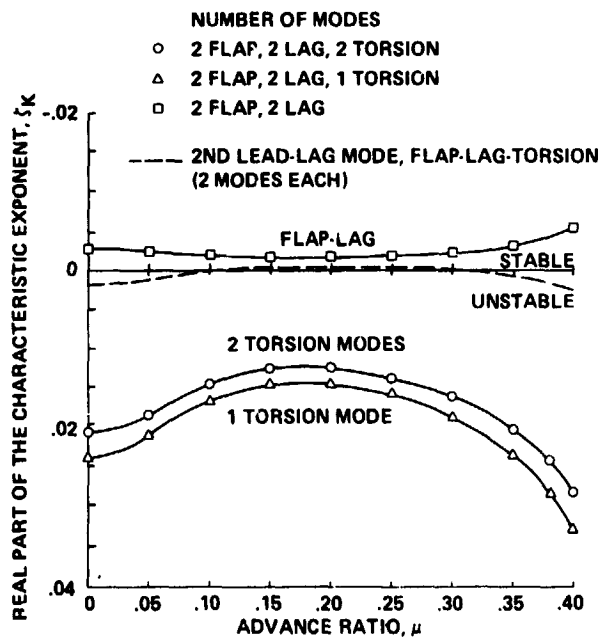


Fig. 9 Lead-lag mode damping versus advance ratio for a flap-lag-torsion model and a flap-lag model: stiff inplane, $\omega_V = 1.4$, $R = 0.0$.

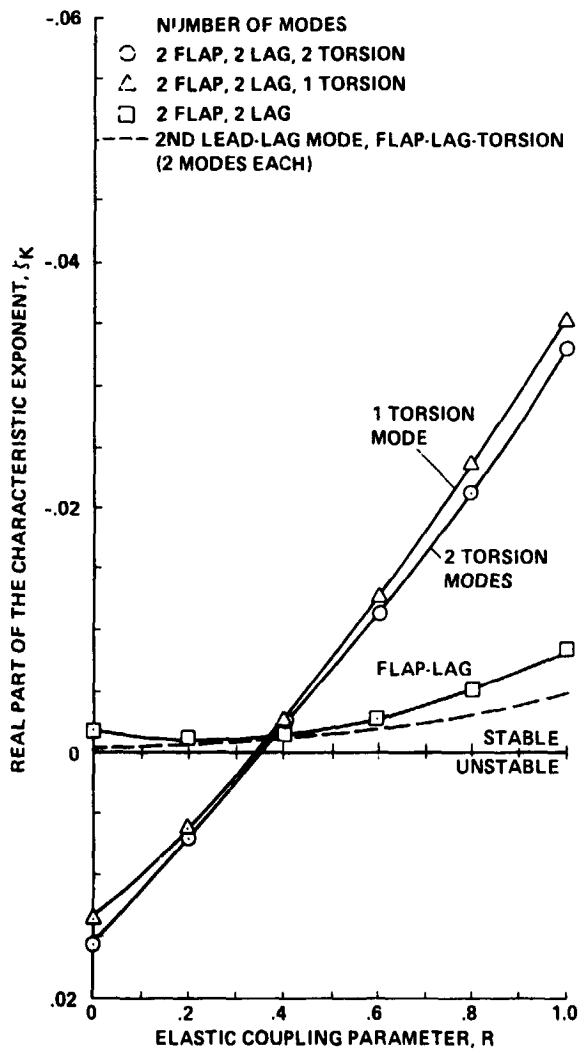


Fig. 10 Lead-lag mode damping versus elastic coupling for a flap-lag-torsion model and a flap-lag model: stiff inplane, $\omega_V = 1.4$, $\mu = 0.25$.

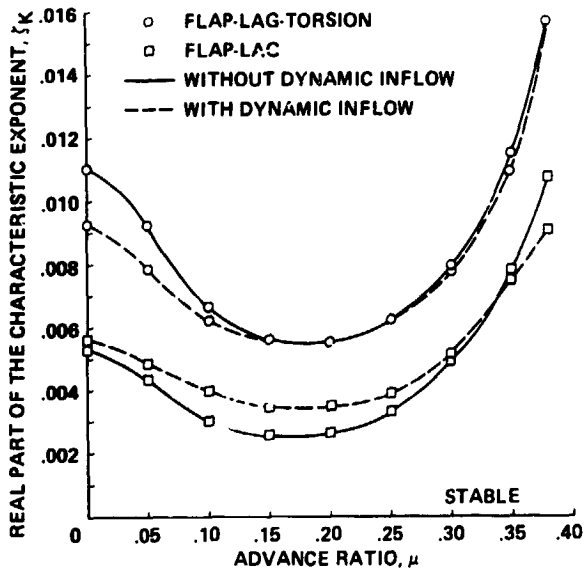


Fig. 11 The effect of torsion and dynamic inflow on lead-lag regressing mode damping versus advance ratio: soft inplane, $\varepsilon_V = 0.7$, $R = 1.0$ (multiblade equations).

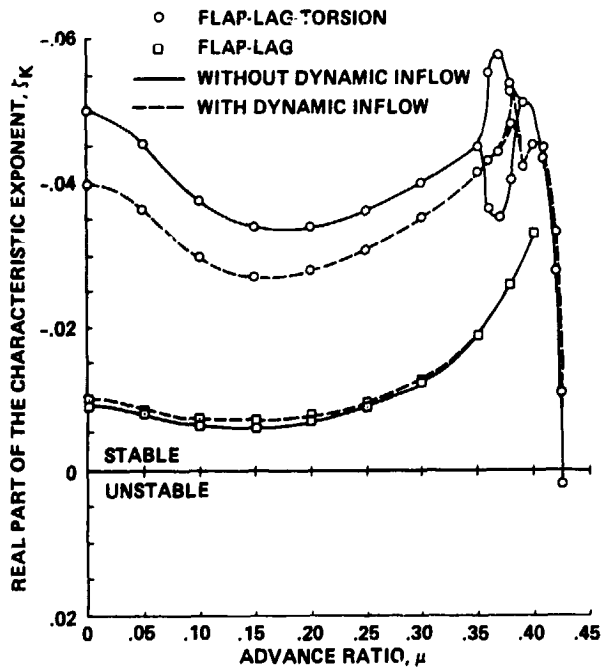


Fig. 13 The effect of torsion and dynamic inflow on lead-lag regressing mode damping versus advance ratio: stiff inplane, $\varepsilon_V = 1.4$, $R = 1.0$ (multiblade equations).

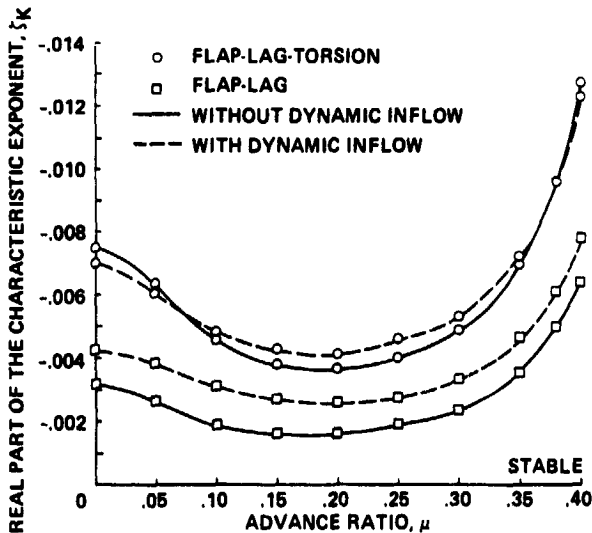


Fig. 12 The effect of torsion and dynamic inflow on lead-lag regressing mode damping versus advance ratio: soft inplane, $\varepsilon_V = 0.7$, $R = 0.0$ (multiblade equations).

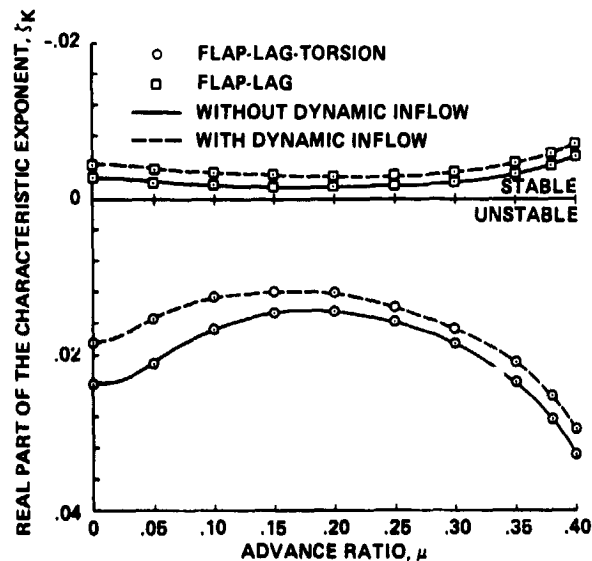


Fig. 14 The effect of torsion and dynamic inflow on lead-lag regressing mode damping versus advance ratio: stiff inplane, $\varepsilon_V = 1.4$, $R = 0.0$ (multiblade equations).

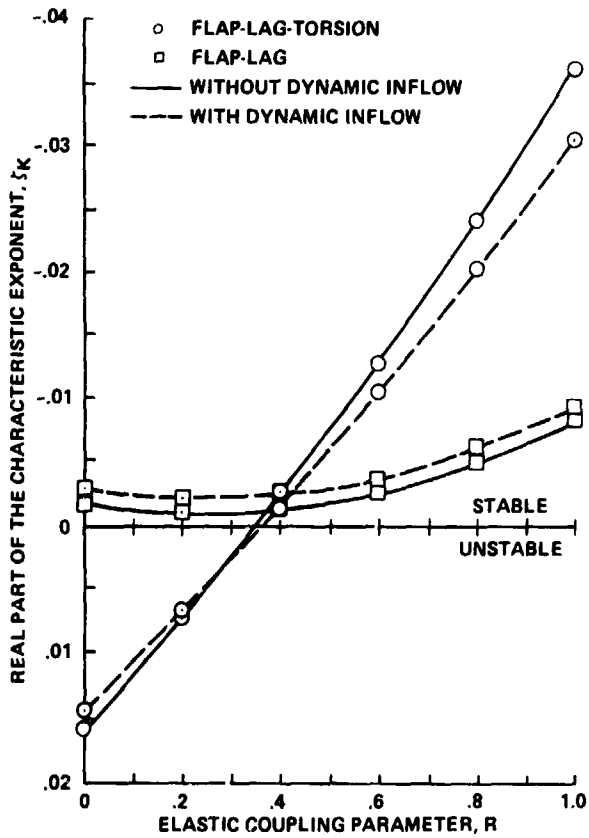


Fig. 15 The effect of torsion and dynamic inflow on lead-lag regressing mode damping versus elastic coupling, stiff inplane, $\omega_v = 1.4$, $\mu = 0.25$ (multiblade equations).

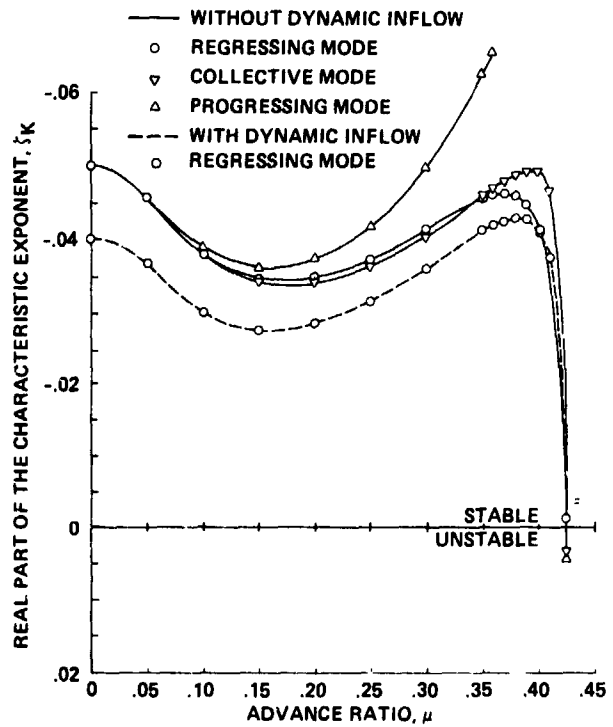


Fig. 16 Comparison of constant-coefficient approximation and Floquet analysis: stiff inplane, $\omega_v = 1.4$, $R = 1.0$ (multiblade equations).

DISCUSSION
Paper No. 15

THE INFLUENCE OF DYNAMIC INFLOW AND TORSIONAL FLEXIBILITY ON ROTOR DAMPING IN FORWARD FLIGHT
FROM SYMBOLICALLY GENERATED EQUATIONS

T. S. R. Reddy
and
William Warmbrodt

Peretz Friedmann, University of California, Los Angeles: I'd like to congratulate you on a very nice paper. Obviously I have a vested interest because for the last three years I have been waiting for somebody to redo the problem to find out whether Kottapalli and I have done it correctly. Now that you have shown these results and Neelakanthan has shown some results at the last European Forum where also the same trends were exhibited I guess I can sleep in peace. What I really wanted to emphasize are two things. One is the contribution you have made is a really significant one because as somebody who has derived equations by hand for a long time I definitely believe that the way to go is to use a computer. The second comment which I have--and it is in the form of a question--is if I correctly understand one results you have shown then it seems to be that dynamic inflow doesn't have an awful lot of influence in the case of coupled flap-lag-torsion in forward flight. I was wondering if you would agree with this statement?

Reddy: Yes, that's what our results show.

Wayne Johnson, NASA Ames Research Center: Following along these lines of what Peretz was discussing about using the computer: In dealing with this subject, if you were going to do the same work, but do it over again were there any pieces of the problem that you did with pencil and paper, [that you] did by hand that if you had to do it all over again you would automate these pieces also. In other words, was there anything left to put into the computer?

Reddy: Yes, we are now finding that the required input data has increased tremendously so we will have to change the program to minimize data inputs.

Friedrich Straub, Hughes Helicopters: How long did it take you to include the forward flight in the equations coming from the hover results?

Reddy: I attended the SDM Conference on the 14th to the 16th of May. Then we came back to this area and submitted the abstract--that was the end of May. We finished the paper by August, but most of this time was spent on developing the trim and response solution program, so it took even less time.

Bill Warmbrodt, NASA Ames Research Center: You might point out that the original derivation was done including the influence of forward flight; however, the program was first exercised to develop the hover results presented at the SDM Conference.